Electrochimica Acta 464 (2023) 142881

Contents lists available at ScienceDirect

Electrochimica Acta

journal homepage: www.journals.elsevier.com/electrochimica-acta

Cell design strategies for sodium-zinc chloride (Na-$ZnCl_2$) batteries, and first demonstration of tubular cells with 38 Ah capacity

Meike V.F. Heinz [a,*], Louis Sieuw [a], Tu Lan [a], Alberto Turconi [b], Diego Basso [b], Fabrizio Vagliani [b], Andrea Pozzi [b], Corsin Battaglia [a]

[a] *Empa, Swiss Federal Laboratories for Materials Science and Technology, 8600 Dübendorf, Switzerland*
[b] *FZSoNick S.A., 6855 Stabio, Switzerland*

ARTICLE INFO

Keywords:
Stationary energy storage
ZEBRA battery
High-temperature metal chloride battery
Molten-salt battery
Molten sodium anode

ABSTRACT

At present, high-temperature sodium-nickel chloride (Na-$NiCl_2$) batteries with nickel-based cathode are produced for specialty markets (e.g. backup power supply) at relatively low volumes. Replacing the nickel in the cathode by cheap and abundant zinc may enable this technology to provide sustainable large-scale energy storage for stationary applications at competitive cost. In this study, we derive design strategies from state-of-the-art Na-$NiCl_2$ cells, and transfer them to Na-$ZnCl_2$ cells. First, we evaluate the influence of cathode compartment filling level, sodium tetrachloroaluminate ($NaAlCl_4$) secondary electrolyte volume, and active metal content on the pressure evolution during battery cell cycling. Based on this evaluation, we define a suitable Zn/NaCl cathode composition for integration into state-of-the-art high-temperature cells with tubular geometry. Second, we present cycling results of Na-$ZnCl_2$ cells with 38 Ah capacity and 0.9 g/cm^2 mass loading, corresponding to an areal capacity of 146 mAh/cm^2 (100% state-of-charge, SOC). During operation at 280–300 °C, tubular cells cycled to high SOC (97–100% SOC) exhibit voltage fading with each cycle. We show that this voltage fading is related to the coarsening and segregation of zinc metal at the cathode, while conductivity and crystalline phase content of the ceramic Na-β''-Al_2O_3 electrolyte are not significantly altered. In contrast, cell voltage and cathode structure remain stable when keeping the cell below 80% SOC. Under these cycling conditions, a cumulative capacity of >550 Ah (22 cycles, 2.1 Ah/cm^2) was transferred at discharge current densities of 10 mA/cm^2 (C/15). Our experiments demonstrate successful integration of zinc electrodes in state-of-the-art tubular cells at commercially relevant mass loadings.

1. Introduction

Several studies have projected low energy costs of 100 – 200 $/kWh for Na-$NiCl_2$ batteries operated at elevated temperatures of ~300 °C [1,2]. Combined with the long design life of 20 years and >4500 cycles of commercial batteries [3], this results in competitive cycle costs of <0.02–0.04 $/kWh/cycle. Even if current production costs do not yet allow reaching these values, this technology shows great potential for large-scale energy storage applications. With respect to scalability, however, the use of nickel should be restricted. Commercial Ni/NaCl cathodes employ significant amounts of this raw material, which may become critical in view of a growing demand [4]. Transition from nickel-based to zinc-based cathodes would provide a sustainable and low-cost energy storage solution, and previous studies already demonstrated the feasibility of sodium-zinc chloride (Na-$ZnCl_2$) cells at laboratory scale [5–8]. Nevertheless, a number of topics still need to be addressed in order to transfer the Na-$ZnCl_2$ electrochemistry to an industrially viable scale.

One important difference between Na-$NiCl_2$ and Na-$ZnCl_2$ cells concerns the aging and state of aggregation of their active cathode materials. While the cathode materials in nickel-based Na-$NiCl_2$ cells are immersed in a molten secondary sodium tetrachloroaluminate ($NaAlCl_4$) electrolyte to enhance transport kinetics at the cathode [9], the active materials (e.g. Ni, NaCl, $NiCl_2$) remain solid up to 350 °C [10]. Although we recently identified electrochemical chlorination and de-chlorination to take part via dissolved cations in Ni/NaCl cathodes [11], the insolubility of metal chlorides in molten $NaAlCl_4$ has often been considered an essential requirement for stable cycling of Ni/NaCl and other sodium-metal halide cathodes [9,12,13]. In Na-$ZnCl_2$ cells, the electrochemical reactions of Zn and NaCl involve intermediate salt

* Corresponding author.
E-mail address: Meike.Heinz@empa.ch (M.V.F. Heinz).

https://doi.org/10.1016/j.electacta.2023.142881
Received 19 January 2023; Received in revised form 13 June 2023; Accepted 12 July 2023
Available online 12 July 2023

melts above 250 °C [6]. Previous studies on Na-$ZnCl_2$ cells even observed an enhanced cycling stability in the presence of liquid active phases at 280 °C, compared to cycling at 240 °C [6]. This was demonstrated using small planar cells of 3 cm^2 active area at a mass loading of 0.3 g/cm^2 (areal capacity 50 mAh/cm^2), where a maximum cumulative capacity of ~1.7 Ah/cm^2 was cycled at a current density of 10 mA/cm^2 (C/5) [6]. In another study on Na-$ZnCl_2$ cells, cumulative cycling reached ~2.8 Ah/cm^2 in planar cells of 4.85 cm[2] active area at 260 °C, enabled by the presence of an additional carbon matrix at the cathode (mass loading <0.6 g/cm^2, 90 mAh/cm^2, up to 33 mA/cm^2, C/3) [8].

While these results from small laboratory-scale cells are promising, information on specific discharge energy and energy efficiency was not reported [5–8], and a quantitative assessment the cycling stability of Na-$ZnCl_2$ cells under realistic operating conditions is presently lacking. Commercial applications require large cells, high Zn/NaCl mass loadings, and a long cycle life in order to compensate the cost contribution of high-temperature cell components and their assembly. State-of-the-art Na-$NiCl_2$ batteries contain tubular cells of 260 cm^2 active area with ~1 g/cm^2 mass loading (150 mAh/cm^2), which are designed to deliver cumulative capacities exceeding 540 Ah/cm^2 (>4500 cycles at 80% depth of discharge) [3,14]. In this geometry, it is vital to assure safe operation, considering that moderate discharge rates of C/3 correspond to high currents of 13 A, 50 mA/cm^2. Commercial Na-$NiCl_2$ cells provide hermetically sealed electrode compartments and an efficient management of molten phases. However, modifications to the cathode composition may affect the stability of the solid, ceramic electrolyte (Na-β''-alumina), which serves as Na-ion conductor, electronic separator, and load bearing structure. While Na-β''-alumina provides excellent mechanical, chemical, and electrochemical stability in Na-$NiCl_2$ batteries, the volume changes of Zn/NaCl electrodes during cycling could affect the mechanical integrity of the ceramic electrolyte [15]. Furthermore, Na-β''-alumina was reported to exchange its Na^+ ions with Zn^{2+} in molten $ZnCl_2$ [16–18], which could compromise ion conductivity and mechanical integrity of Na-$ZnCl_2$ cells.

In this study, we integrate Zn/NaCl cathodes in state-of-the-art tubular cells. Based on cell geometry and electrode design at commercial scale, we define Ni/NaCl and Zn/NaCl model electrodes with a suitable combination of mass loading and composition. We assemble tubular Na-$ZnCl_2$ cells with 38 Ah capacity and demonstrate how operating temperatures between 240 °C and 420 °C, charge rates between C/29 and C/5 (5 – 31 mA/cm^2), and cut-off voltages between 1.65 V and 2.35 V affect the evolution of cell voltage, cycled capacity, and stability of cell components.

2. Materials and methods

To prepare cathode granules with 30% active zinc content, 65.1 wt% Zn (4.5 μm average particle size, Ultrapure zinc dust UP4, Purity Zinc Metals, USA) and 34.9 wt% NaCl (microfine/milled, 88 wt% < 45 μm, 99.1–99.4% purity) were roll mixed for 4 h The resulting powder mix (~2 kg batch size) was compacted at a roll force of 35 kN (Komarek B050A) before granulation (Komarek G100SA granulator). After granulation, coarse particles >1.6 mm were removed by sieving, and the fine fraction < 212 μm was adjusted at 2.6 wt%. This provided granules with a suitable tap density for $NaAlCl_4$ vacuum infiltration (1.85 g/cm^3). Using a vibrating table, 237 g Zn-based cathode granules were inserted manually into empty tubular high-temperature cells (see SI section A; cathode loading 146 mAh cm^{-2}). These cells were then re-introduced to the state-of-the-art production flow of high-temperature cells at FZSoNick, including injection of the molten $NaAlCl_4$ electrolyte (116 g) at 200 °C and cell sealing by laser welding in the production line (SI section B). After wiring, cell cycling was performed in a furnace with individual thermocouples for each cell. In all experiments, constant-current (CC) and constant-voltage (CV) routines were applied both during charge and discharge (current limitation at 0.7 ± 0.1 mA/cm^2), as common for sodium-metal chloride batteries. Stable CC—CV cycling in a defined SOC range corresponds to coulombic efficiencies of 100%. Therefore, we discuss the cell performance in terms of charge/ discharge time, discharge energy, and energy efficiency. Energy density was computed as the time integral of cell voltage times current during charge and discharge, divided by the mass of cathode granules.

For postmortem analysis, the cycled cells were disassembled in the discharged state at room temperature, and the cell case was carefully cut open. The tubular electrolyte was retrieved, which contained the cathode granules, secondary $NaAlCl_4$ electrolyte, nickel current collector wires, and a carbon felt. Sections were cut at different heights of tube using a water-cooled diamond blade cutter. Pictures of the tube sections were taken immediately after cutting, as $NaAlCl_4$ reacted with the cooling water. One tube section (~30 mm wide) was cleaned, and electrical contacts were applied to the cut surfaces (Aquadag colloidal graphite mixed with aqueous $NaNO_3$/$NaNO_2$, graphite discs, sheets of silver welded to silver wires). This geometry was used to measure the resistance of the Na-β''-alumina electrolyte along its height in a furnace at different temperatures (alternating current signal at 9 kHz, 10 mA and 20 mA). The contact area of the cloverleaf-shaped electrolyte section was determined from its weight, density (3.20 g/cm^3), and height to derive the Na-β''-alumina conductivity. Another electrolyte tube section was crushed into powder (D50 50–100 μm) for X-ray powder diffractometry.

3. Theory: cell design strategies

In order to design successful sodium-zinc chloride (Na-$ZnCl_2$) cells, it is important to consider the rationale of cell and electrode design employed in commercial Na-$NiCl_2$ batteries. Na-$NiCl_2$ battery cells are based on a solid, ceramic electrolyte (Na-β''-alumina), which separates the molten sodium anode from the metal/ metal chloride cathode (Fig. 1a). The tubular geometry of commercial Na-$NiCl_2$ cells provides available electrode compartment volumes of approximately 150 cm^3 at the cathode, and 75 cm[3] at the anode (corrected for relevant passive components, such as current collectors and shims to manage molten phases). Cells are assembled in the discharged state, with rock salt and nickel powders as main electrode constituents [13]. This avoids the handling of highly reactive sodium metal at the anode, and of hygroscopic as well as toxic metal chlorides at the cathode. Commercial Na-$NiCl_2$ cells further contain iron and a number of different additives, which serve to activate and stabilize the cathode processes [13,19]. The solid cathode materials are granulated to enable automated electrode filling, without further needs for compaction inside the cell [13]. Immersion of the solid active materials in a secondary electrolyte (molten $NaAlCl_4$) enhances transport kinetics at the cathode [9]. The liquid sodium metal anode, which provides high specific capacity (1166 mAh/g) and excellent rate-capability [20], is generated electrochemically during the first (maiden) charge. Commercial Na-$NiCl_2$ batteries feature cells of significant size (38–40 Ah, 260 cm[2]) and cathode loading (~1 g/cm^2, Fig. 1b) [3]. Related to the high areal capacity of ~150 mAh/cm^2, discharge at a high current density of 50 mA/cm^2 translates to relatively low C-rates of C/3 in this geometry, which are typical for commercial Na-$NiCl_2$ batteries. Upon charge, the transition metals (Ni, Fe) react to solid transition metal chlorides at the cathode ($NiCl_2$, $FeCl_2$), while forming molten sodium at the anode [19]. As the conversion to metal chloride locally passivates the metal surface [21], the electrochemical reactions proceed along a reaction front through the thick cathode (0.5–1.0 cm), moving away from the electrolyte surface during each half cycle [22]. To maintain electronic conductivity in the electrode at all states of charge (SOC), nickel is applied in excess quantities at the cathode. Typically, the active metal content used for electrochemical cycling is only about 30% [19]. Together with the presence of additives, this reduces the gravimetric capacity of state-of-the-art nickel and iron chloride electrodes from >300 mAh/g to 160 mAh/g (Fig. 1b). Presently, production costs for Na-$NiCl_2$ batteries amount to 300–350 €/kWh at battery pack level. Major cost factors are the price and amount of

a)

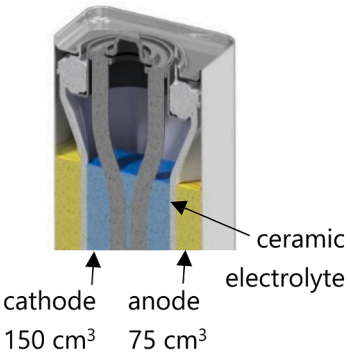

b) **State-of-the-art Na-NiCl2 cells (mixed Ni,Fe/NaCl cathode)**

cell capacity	[Ah]	38-40
cell active area	[cm²]	260
nominal discharge capability, C/3	[mA/cm²]	50
cathode loading	[g/cm²]	1.0
cathode thickness	[cm]	0.5-1.5
capacity (incl. additives, excl. $NaAlCl_4$)	[mAh/g]	160
current production	[MWh/year]	25
production cost (battery pack)	[€/kWh]	300-350

Fig. 1. Design and properties of state-of-the-art Na-$NiCl_2$ battery cells. a) Electrode compartment geometry and available electrode volumes. b) Cell characteristics, including capacity, cathode loading, and production cost.

nickel required at the cathode, as well as cell production cost [6,23]. Furthermore, Na-$NiCl_2$ batteries are currently produced for specialty market applications, such as backup power application, at relatively low volumes of 25 MWh/year by FZSoNick in Switzerland. Adoption of a Zn/NaCl cathode, combined with a re-evaluation of the cell design strategy, offers potential to reduce the cost of this technology.

When inserting Zn/NaCl cathodes in state-of-the-art tubular high-temperature cells, we need to consider the mechanical stresses evolving during cell operation. The underlying electrochemical conversion reactions, as well as temperature variations, entail considerable volume changes of the electrode materials at different SOC, which are compensated by the presence of inert gas volumes at the top of the cells (Fig. 1a). For a given cell geometry, these volume changes convert to pressure differences between the hermetically sealed electrode compartments, which can lead to critical stresses on the ceramic electrolyte [15]. Similar to Na-$NiCl_2$ batteries, the electrochemical conversion reaction of Zn and NaCl to $ZnCl_2$ and Na provides a gravimetric capacity of 294 mAh/g (Eq. (1)).

$$Zn + 2NaCl \leftrightarrow ZnCl_2 + 2Na \quad \text{(Eq. 1)}$$

$$Zn + 2\,NaCl \leftrightarrow Zn^{2+}Cl_2 + 2\,Na^+ + 2\,e^- \text{ (positive electrode, cathode)}$$

$$2\,Na^+ + 2\,e^- \leftrightarrow 2\,Na \text{(negative electrode, anode)}$$

According to thermodynamic phase calculations, this reaction takes place via solid Na_2ZnCl_4 as intermediate phase, further involving Zn^{2+}-containing salt melts at temperatures above 250 °C [6,7]. For simplicity, we here focus on full conversion between 0% SOC (Zn + 2 NaCl) and 100% SOC ($ZnCl_2$ + 2 Na), corresponding to the end states of this reaction. This provides a basis to design the composition and capacity of tubular Na-$ZnCl_2$ cells, as the volume of cathode materials decreases from a maximum at 0% SOC to a minimum at 100% SOC, while that of the anode increases with the generation of sodium in both Na-$NiCl_2$ and Na-$ZnCl_2$ cells. This results in an overall decrease in volumetric capacity from 822 mAh/cm³ to 537 mAh/cm³ at 300 °C (Figure 2a; see supplemental information SI section C, for the thermal expansion coefficients and temperature dependent densities). In Fig. 2b, we illustrate the evolution of gravimetric and volumetric capacity of Zn/NaCl electrodes with variable active Zn content. A realistic active metal content of 30% corresponds to a theoretical capacity of 160 mAh/g, corresponding to the specific capacity available in state-of-the-art Na-$NiCl_2$ cells comprising Ni, Fe, and additives. The capacity of pure Ni/NaCl electrodes with 30% active metal content is slightly higher (172 mAh/g), due to the lower molar mass of Ni and $NiCl_2$, compared to Zn and $ZnCl_2$. To assess the total weight and volume of Zn/NaCl and Ni/NaCl electrodes, we further include the presence of the secondary electrolyte, $NaAlCl_4$. To fill the porosity of the solid cathode materials at a realistic packing density, we consider the presence of 50 vol% molten $NaAlCl_4$ at 300 °C (see Fig. 2b). The effect of variable $NaAlCl_4$ contents on gravimetric and volumetric capacity at a constant active metal content of 30% is displayed in Fig. 2c. Based on this, we define Ni/NaCl and Zn/NaCl model electrode compositions X_{Ni} and X_{Zn}, both comprising an active metal content of 30%, and 50 vol% molten $NaAlCl_4$ at 300 °C (Fig. 2c, composition in SI section D). The theoretical capacity of these model electrodes, including $NaAlCl_4$, amounts to 123 mAh/g for

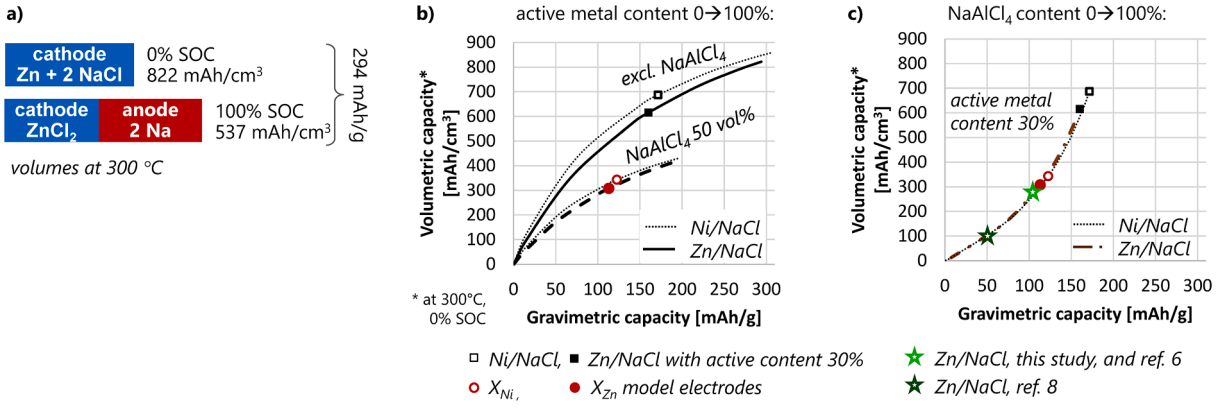

Fig. 2. a) Volume and specific capacity of Zn/NaCl electrodes at 0% and 100% SOC, 300 °C. b) Volumetric and gravimetric capacity of Zn/NaCl and Ni/NaCl electrodes with variable active metal content; excluding $NaAlCl_4$, and including 50 vol% $NaAlCl_4$ content. c) Volumetric and gravimetric capacity of Zn/NaCl and Ni/NaCl electrodes with 30% active metal and variable $NaAlCl_4$ content. Results for the Ni/NaCl and Zn/NaCl model electrodes, X_{Ni} and X_{Zn}, as well as experimental results from this study and from literature are included for comparison.

Ni/NaCl, and 113 mAh/g for Zn/NaCl. Experimental compositions applied in Na-$ZnCl_2$ cells in the second part of this study, as well as from literature [6,8], are indicated in Fig. 2c for comparison. In general, Fig. 2b shows that increasing the active metal content from 30% towards 100% has a stronger effect on gravimetric than on volumetric capacity. This is because increasing amounts of NaCl with relatively low density ($\rho_{NaCl,300\ °C} = 2.09$ g/cm^3) are required for the electrochemical reaction, together with the active metal ($\rho_{Zn,300\ °C} = 6.96$ g/cm^3). In contrast, considering also $NaAlCl_4$ in the specific capacities ($\rho_{NaAlCl4,300\ °C} = 1.60$ g/cm^3), a reduction in molten salt content strongly improves the volumetric capacity, with a milder effect on gravimetric capacity.

In order to investigate the influence of cathode composition and cell geometry on cell capacity and pressure variation, we represent state-of-the-art Na-$NiCl_2$ cells in a simplified cylindrical geometry in Fig. 3a. At a cell height of 22 cm, the available electrode volumes of 150 cm[3] and 75 cm[3] translate to an average radial thicknesses of ≈1.5 cm for the cathode, and ≈0.3 cm for the anode. In Figure 3b-c, we present the volume evolution of the model cathodes X_{Ni} and X_{Zn}, assuming a compartment filling level of 90 vol% at the cathode (at 300 °C, 0% SOC; anode and remaining cathode volume are filled with inert gas). Due to a higher density and lower molar volume of Ni compared to Zn, the Na-$NiCl_2$ model cell hosts a capacity of 46.4 Ah, while that of the Na-$ZnCl_2$ cell is 10% lower (41.5 Ah). In both cases, electrochemical conversion entails a linear increase of the sodium anode volume upon charge (+0.974 cm^3/Ah), while the volume of cathode materials decreases between 0% SOC and 100% SOC (-0.47 cm^3/Ah for Na-$NiCl_2$, −0.33 cm^3/Ah for Na-$ZnCl_2$). As previously derived [15], the corresponding changes in gas volumes at anode and cathode ($V_{g,a}$, $V_{g,c}$) result

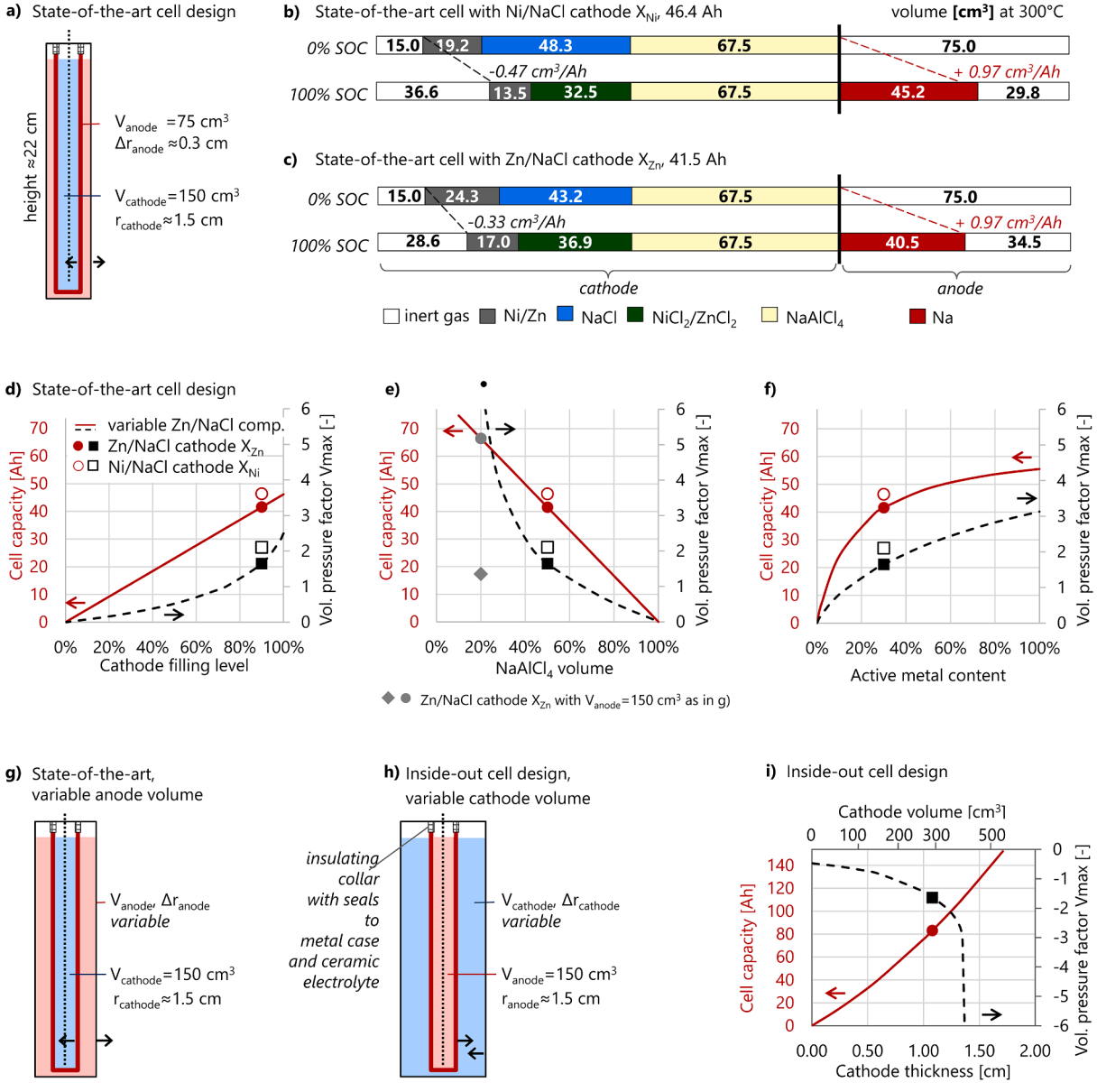

Fig. 3. a) Representation of state-of-the-art Na-NiCl2 cell design, with cathode placed inside of ceramic electrolyte tube, and sodium anode contained by the outside metal cell case. Volume change of electrode materials with SOC for b) Ni/NaCl model cathode XNi and c) Zn/NaCl cathode XZn at 300 °C. Cell capacity and volumetric pressure factor Vmax, of state-of-the-art cells with variable d) cathode filling level, e) NaAlCl4 vol, and f) active metal content (all at 300 °C). Only one parameter is varied, values for Ni/NaCl cathode XNi and Zn/NaCl cathode XZn are indicated (90 vol% cathode filling level, active metal content 30%, NaAlCl4 vol 50%). g) Representation of cell design with variable anode compartment volume. h) Inside-out cell design with sodium anode inside of ceramic electrolyte tube, and cathode of variable thickness contained by the outside metal case. i) Cell capacity and volumetric pressure factor Vmax, of inside-out cells with variable cathode thickness and volume. The geometry of ceramic electrolyte, insulating collar, and seals remains the same in a,g,h); the legend in d) applies to d-f,i).

in a maximum pressure difference Δp_{max} between 0% SOC (state 1) and 100% SOC (state 2) according to:

$$\Delta p_{max} = p_1 \frac{T_2}{T_1}\left(\frac{V_{g,a1}}{V_{g,a2}} - \frac{V_{g,c1}}{V_{g,c2}}\right) = p_1 \frac{T_2}{T_1} V_{max}. \quad \text{(Eq. 2)}$$

This shows that, independent of electrode composition and cell geometry, a reduction in cell pressure p_1 during assembly at 0% SOC directly reduces Δp, providing great potential to tune pressure and thus stress evolution. Similarly, sealing of the cells at the operating temperature (e.g. $T_1 = T_2 = 300$°C) reduces the temperature factor $\frac{T_2}{T_1}$ from 1.92 to 1.00, compared to sealing at 25°C. Furthermore, the filling level of cathode and anode compartment with electrode materials needs to be designed to reduce the volumetric pressure factor $V_{max} = \left(\frac{V_{g,a1}}{V_{g,a2}} - \frac{V_{g,c1}}{V_{g,c2}}\right)$ in Eq. (2), relating the inert gas volumes present at anode and cathode at 0% SOC and 100% SOC. For cell closure at ambient pressure and operating temperature, the value of V_{max} corresponds to the absolute pressure difference between the electrode compartments in atmospheres. Based on Eq. (2), a state-of-the-art tubular cell with the Zn/NaCl cathode X_{Zn} features a lower volumetric pressure factor (V_{max}=1.65) than one with Ni/NaCl cathode X_{Ni} (V_{max}=2.11). This translates to lower pressure differences of up to 1.67 bar in corresponding Na-$ZnCl_2$ cells, compared to 2.14 bar in Na-$NiCl_2$ cells. The detailed effects of variable cathode filling level, $NaAlCl_4$vol, and active metal content on theoretical cell capacity and maximum volumetric pressure factor V_{max} in state-of-the-art cells are summarized in Fig. 3d-f. While a further increase of the cathode filling level towards 100 vol% linearly increases the capacity of Na-$ZnCl_2$ cells towards 46.1 Ah, this goes in hand with a steep rise of the volumetric pressure factor V_{max} (Fig. 3d). Similarly, a decrease in $NaAlCl_4$ content at the cathode linearly increases the cell capacity, but again at the cost of strongly increasing V_{max} (Fig. 3e), with a negative effect on the mechanical stability of the ceramic electrolyte. For the given cell geometry, increasing the active metal content is an option to increase the cell capacity at a moderate increase of V_{max} (Fig. 3f). Please note that the full range of compositions addressed here severely challenges the microstructural requirements in electronic percolation and fast ion transport through the cathode. Thus, only certain compositional ranges are likely to find a practical implementation with suitable microstructure. Overall, the cell with model cathode X_{Zn} represents a good compromise between capacity and pressure evolution in the state-of-the-art cell geometry.

Another option to significantly increase the cell capacity, and thus to reduce cell production costs for stationary storage application, is to adopt a different cell design. Increasing the dimensions of the ceramic Na-β''-alumina electrolyte and its hermetic seals to the metal case is technically challenging, adding additional cost. Instead of increasing length and diameter of a tubular ceramic electrolyte, the compartment volume of the outer electrode can also be increased by shaping the outside metal cell case, thus increasing its volume and reducing the volumetric pressure factor V_{max} (Fig. 3g). For example, a theoretical increase in cell capacity to 66.4 Ah by the decrease of the $NaAlCl_4$vol to 20% in the state-of-the-art design would entail a volumetric pressure factor V_{max} of 6.90, compromising the mechanical stability of the cell. However, doubling the anode compartment volume to 150 cm^3 would reduce V_{max} to 1.35 for the same composition and cell capacity (Fig. 3e). Another design option is to employ an inside-out cell geometry, where the molten sodium anode is located inside the ceramic Na-β''-alumina electrolyte tube, while the cathode materials are contained by the outer metal cell case. This enables integration of variable cathode thicknesses at a larger anode volume of 150 cm^3. Based on the volume of sodium, this doubles the upper limit of the cell capacity from 77 Ah to 154 Ah, without changing the size of the ceramic Na-β''-alumina electrolyte, its seals, and the insulating collar (Fig. 3h). As indicated by arrows, the volume and pressure evolution in the inside-out geometry is opposite to that in the state-of-the-art cell design. The corresponding evolution of cell capacity and volumetric pressure factor V_{max} with outside cathode volume and thickness and volume is displayed in Fig. 3i. According to Eq. (2), the inside-out cell geometry can provide twice the capacity of state-of-the-art cells at the same magnitude of V_{max}, when the outside electrode compartment is doubled (e.g. $V_{cathode}$= 300 cm^3, cathode composition X_{Zn}, cell capacity 83.1 Ah at $|V_{max}|$=1.65). This design option is already successfully applied in commercial sodium-sulfur cells [24]. For Na-$NiCl_2$ cells, however, an inside-out cell geometry is not considered cost-efficient. This is because iron oxidation during operation at ~2.5 V would lead to electrochemical corrosion of steel-based cell casings, requiring them to be made from more noble metals. In contrast, the lower voltage of Na-$ZnCl_2$ cells avoids this degradation mechanism, providing a promising design option. Nevertheless, further investigations on the (electro-)chemical stability of steel-based metal casings with the cathode materials [25] and with molten $NaAlCl_4$ in Na-$ZnCl_2$ cells are required before implementing the inside-out cell geometry in large tubular cells.

4. Results and discussion: Na-$ZnCl_2$ cycling in state-of-the-art tubular cells

Based on the cell design strategies discussed above, we prepared additive-free cathode granules with an active zinc content of 30% (65.1 wt% Zn, 34.9 wt% NaCl). At a tap density of 1.85 g/cm^3, the standard filling level in state-of-the-art tubular high-temperature cells was reached at a mass loading of 237 g (0.91 g/cm^2 at an active cell area of 260 cm^2), resulting in a theoretical cell capacity of 37.9 Ah (146 mAh/cm^2). These cells were then re-introduced to the state-of-the-art production flow of Na-$NiCl_2$ cells. 116 g of molten $NaAlCl_4$ electrolyte were injected (54 vol% at 300 °C; cathode filling level 89.5%), and the cells were sealed in the production line at >200 °C under ambient pressure. To evaluate how operating temperature, charge/discharge rate, and cut-off voltages affect the available capacity and cell voltage, we prepared three tubular Na-$ZnCl_2$ cells. In all experiments, we applied constant-current (CC) followed by constant-voltage (CV) routines during charge and discharge (current limitation at 0.7 ± 0.1 mA/cm^2), as common for sodium-metal chloride batteries.

For the tubular Na-$ZnCl_2$ cell #1, we performed a run-in procedure at variable temperatures to activate the full capacity (37.9 Ah, 100% SOC; see Fig. 4a, cycle 1–4). The maiden charge was conducted at 280 °C, C/29 (1.3 A) with 2.1 V upper cut-off voltage. This procedures charged only 52% of the theoretical capacity (19.9 Ah), which was mostly available for discharge at C/10 (19.5 Ah at 4 A, 1.8 V lower cut-off). For the second cycle, we decreased the operating temperature to 240 °C. Due to an increase in cell resistance at the lower temperature, we could access only 37% of the capacity (13.9 Ah, lower cut-off voltage 1.65 V). In a third cycle at 300 °C, we slightly increased the upper cut-off voltage and successfully performed a full charge (100% SOC, 37.9 Ah; upper cut-off at 2.25 V), followed by discharge over 84% SOC (32.0 Ah). In a fourth cycle, we tripled the charge rate (to C/10, 4 A) and doubled the discharge rate (to C/5, 8 A). Charging to 100% SOC was possible. Discharge to a lower cut-off voltage of 1.70 V covered only 80% SOC, and both charge and discharge proceeded at the voltage limitations over 20–25% SOC at the higher rates.

After these run-in cycles, we performed regular cycling experiments at 300 °C over 80% SOC (30.3 Ah), with charge and discharge rates of C/10 between 1.65 V and 2.30 V (Fig. 4b, cycle 5–14; 5th charge curve not recorded due to a technical problem). During charge, the CV mode was reached in all cycles. While the charged capacity was constant (~79% SOC, 29.8 ± 0.2 Ah), it remained slightly below the target value in all regular cycles. As the target capacity (80% SOC, 30.3 Ah) was discharged in all cycles, this shifted the capacity range to lower SOC values with each cycle (e.g. from 20–100% SOC in cycle 5 to 10–90% SOC in cycle 14, Fig. 4c). In terms of coulombic efficiency, this corresponds to values exceeding 100% in all regular cycles for this cell (see SI section E). The cell voltage continuously increased with each cycle during CC charge, and decreased during CC discharge (voltage hysteresis), but with

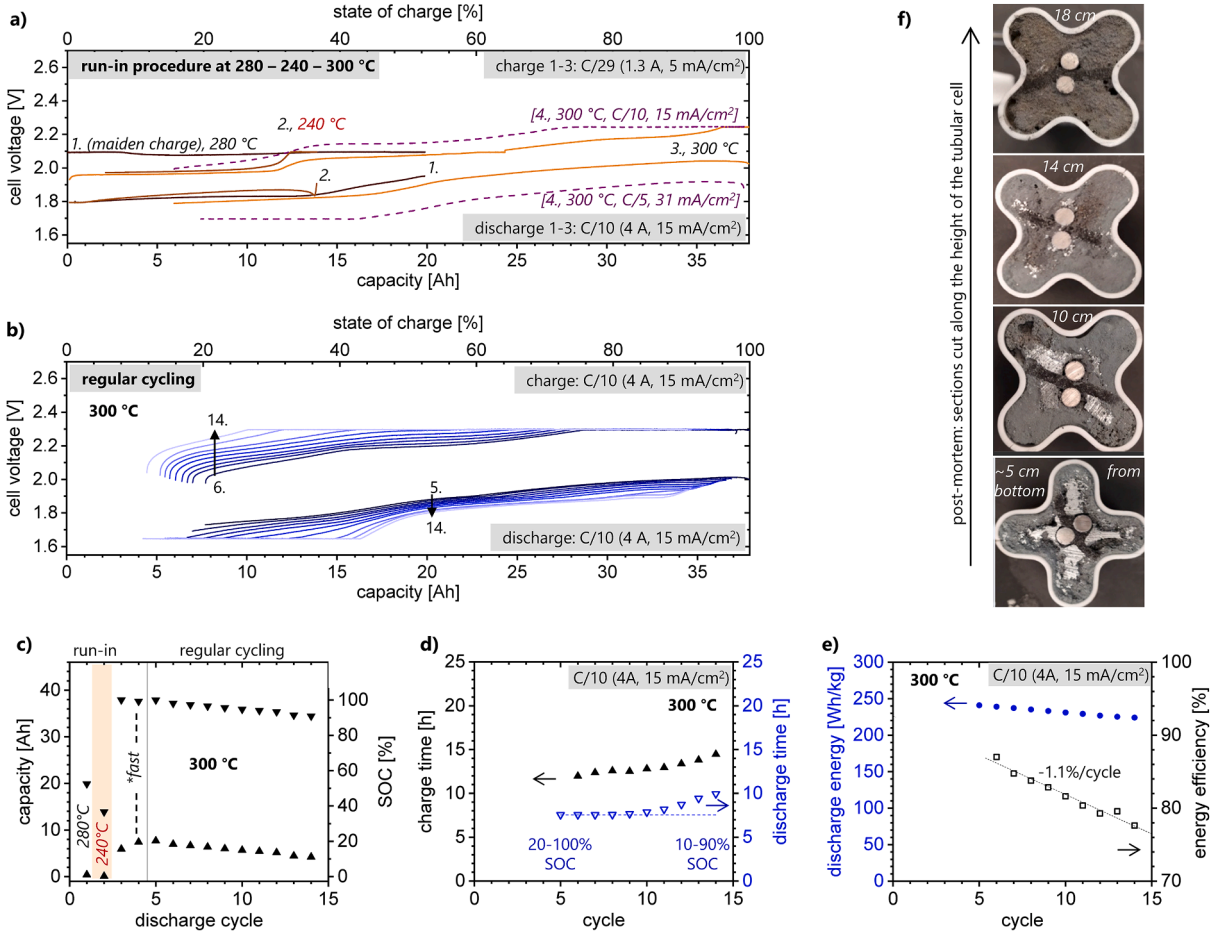

Fig. 4. Cycling of tubular Na-$ZnCl_2$ cell #1 (37.9 Ah) at 300 °C between 1.65 and 2.10–2.30 V, cumulative capacity ~400 Ah (>1.5 Ah/cm^2). a) The first three run-in cycles at 280 °C, 240 °C and 300 °C activate the full capacity (100% SOC, 37.9 Ah). A fourth cycle at higher rates (charge at C/10, discharge at C/5) over 84% SOC reaches the voltage limitations over 20–25% SOC. b) In 10 consecutive regular cycles (5–14), the charged capacity remains slightly below the target of 80% SOC (30.2 Ah). c) As a result, the start and end capacities are shifted to lower SOC values. Due to a continuous increase in cell resistance, the d) charge times increase from 12.0 to 14.5 h, and the discharge times increase from the CC limit of 7.6 h to 9.9 h during regular cycling. e) The corresponding discharge energies and energy efficiencies decrease from -241 to −221 Wh/kg, and from 87% to 78%. f) After cycling, the ceramic electrolyte tube is intact without visible signs of degradation. However, segregation of zinc metal occurs at the cathode, which accumulates towards the bottom and center of the cell (bright, shiny regions).

a different magnitude depending on SOC (arrows in Fig. 4b). This indicates that cathode processes govern the corresponding increase in cell resistance. These are influenced by a reaction-front mechanism [22], and/or to the formation of intermediate phases and salt liquids at the Zn/NaCl cathode [6]. As a result, the charge time increased from 12.0 to 14.5 h (Fig. 4d). Discharge occurred in CC mode over 7.6 h in the first three cycles, but gradually increased to a discharge time of 9.9 h in the 14th cycle. The discharge energy decreased from 241 Wh/kg to 221 Wh/kg during regular cycling (cycle 5–14). The corresponding energy efficiency decreased by 1.1%/cycle, from 87% to 78% (Fig. 4e).

After cycling a cumulative capacity of ~400 Ah (>1.5 Ah/cm^2), cell #1 was disassembled in the discharged state. The ceramic Na-β''-alumina electrolyte did not show visible signs of degradation, and sections were cut at different heights of the tubular cell (~5 cm, 10 cm, 14 cm, and 18 cm from the bottom of the ~23 cm long cell). The corresponding sectional views (Fig. 4f) show the cathode material (Zn/NaCl granules and $NaAlCl_4$), with two nickel-rod current collectors at the center, and a carbon felt serving as $NaAlCl_4$ reservoir. The cathode material revealed significant segregation, with increasing amounts of Zn metal aggregated at the bottom of the cell (in height), and towards the center of the cloverleaf-shaped cathode. The conductivity of the ceramic Na-β''-alumina electrolyte, measured along the height of a tube section, was the same as that of pristine samples (0.2 S/cm at 300 °C, Fig. 5,

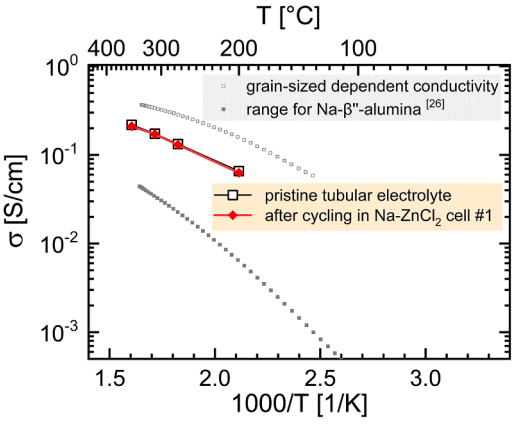

Fig. 5. The electrical conductivity of the ceramic Na-β''-alumina electrolyte in tubular Na-$ZnCl_2$ cell #1 corresponds to that of pristine sample (0.2 S/cm at 300 °C) after cycling (cumulative capacity >1.5 Ah/cm^2).

grain-size dependent conductivity of Na-β''-alumina plotted for reference [26]). This confirms that degradation of the cathode material dominated the voltage fading of Na-$ZnCl_2$ cell #1. The corresponding

microstructural changes reduce the surface area of active materials, impair homogeneous electronic percolation through the metal backbone, and deteriorate ion transport through $NaAlCl_4$ at the cathode. This increases the cell resistance, causes a gradual increase in cell overpotentials (Fig. 4b), and translates into a decrease in energy efficiency by ~1% at C/10 (10 mA/cm^2) for cell #1.

For cell #2, we increased the cut-off voltages by +50 mV (1.70 V - 2.35 V) to facilitate charging to 100% SOC during regular cycling. Applying a similar run-in procedure at 300 °C, 240 °C and 300 °C, the cell was charged to 97% SOC (36.6 Ah) in the third cycle (Fig. 6a). Similar to cell #1, we then performed regular cycling at 300 °C, C/10, but with a slightly increased SOC range of 84% SOC (32 Ah) to increase the energy density (Fig. 6b, cycle 4–8). With these conditions, the cycled capacity stabilized at a constant SOC range between 12% and 96% SOC (Fig. 6c). At the increased cut-off voltages, the charge times were lower than for cell #1 (10.5–11 h), and discharge proceeded in CC mode over 8.0 h for all cycles (Fig. 6d), despite a wider SOC range (84% vs. 80%). Although the voltage profiles of cell #1 and cell #2 were very similar after the run-in procedure, cell #2 showed a smaller voltage hysteresis than cell #1 during regular cycling (see SI section F for a direct comparison of voltage profiles). This indicates differences in the evolution of cell resistance, which we ascribe to microstructural effects. These could be caused by small differences in the cycling conditions applied (cut-off potentials, resulting SOC range), but also statistical variations in the cathode microstructure could play a role.

Nevertheless, the evolution of cell voltage again indicated an increase in cell resistance with each cycle (Fig. 6b, cycle 4–8). As a result, the discharge energy decreased from 261 Wh/kg to 255 Wh/kg (Fig. 6e). The corresponding energy efficiency decreased by 1.0%/cycle, from 91% to 87%. Thus, a combination of lower cell resistance and increased cut-off voltage in cell #2 enhanced its performance, compared to the cell #1. However, it still showed voltage and efficiency fading with each cycle, similar to cell #1.

To evaluate if further degradation of Na-$ZnCl_2$ cells could lead to dangerous conditions, we then increased the operating temperature to the melting point of zinc metal at 420 °C, simulating cell failure due to overheating (Fig. 6b, cycle 9–13). Unexpectedly, the first charge at this temperature significantly exceeded the theoretical capacity limit, reaching up to 115% SOC (43.7 Ah) at a cut-off voltage of 2.35 V. Furthermore, over a wide range of SOC, both the charge and discharge voltages at 420 °C were lower than at 300 °C. These observations indicate the presence of additional electrochemical reactions at lower voltage, which provide additional capacity at this temperature. This could be related to partial electrochemical consumption of $NaAlCl_4$, as previously described for Na-$NiCl_2$ cells [9,13,27]. Nevertheless, the cell successfully continued cycling at 420 °C for five cycles, providing discharge energies of 254±1 Wh/kg at energy efficiencies of 85% (after stabilizing the SOC range, cycle11–13). No catastrophic cell failure

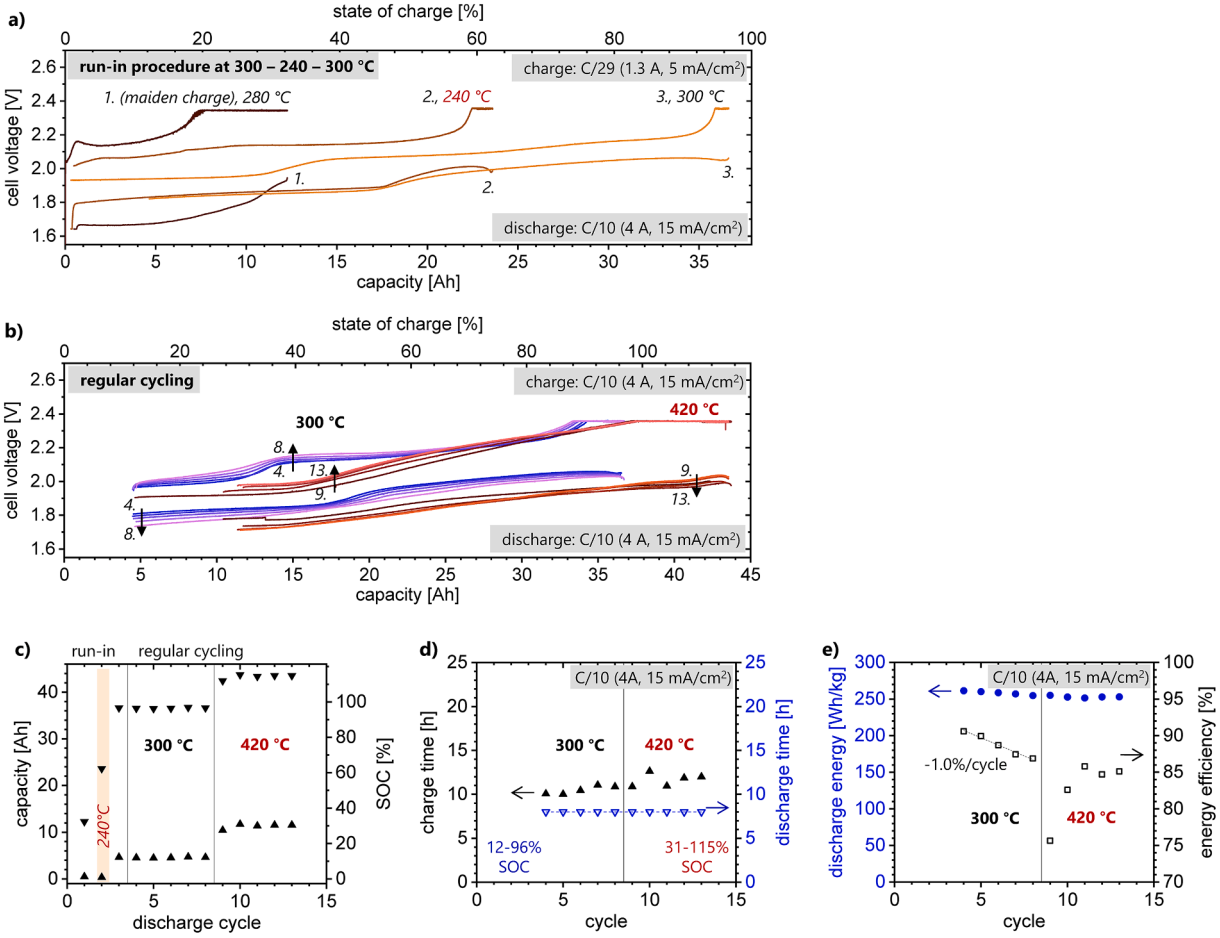

Fig. 6. Cycling of tubular Na-$ZnCl_2$ cell #2 (37.9 Ah) at 300 °C and 420 °C between 1.70 and 2.35, cumulative capacity ~390 Ah (1.5 Ah/cm^2). a) The first three run-in cycles at 300 °C, 240 °C and 300 °C activate almost the full capacity (97% SOC, 36.6 Ah). b) During regular cycling at 300 °C, C/10 (cycle 4–8) the targeted charge/discharge range of 84% SOC (32 Ah) is met, and c) the cycled capacity stabilizes between 12% SOC and 96% SOC. After increasing the operating temperature to 420 °C in consecutive cycles (9–13), the cell is overcharged (capacities between ~30% and 115% SOC), but no catastrophic failure occurs. d) Charge and discharge times amount to 10.0–12.5 h and 8.0 h, respectively. e) The corresponding discharge energies at 300 °C decrease from 261 to 254 Wh/kg. Similar to cell #1, the energy efficiency decreases by −1.0/cycle, from 91% to 87%.

occurred, and the percolating metal backbone was not compromised during five consecutive cycles 420 °C. However, after reaching a cumulative capacity of ~390 Ah (1.5 Ah/cm^2) and cooling down to room temperature over a weekend, cycling could not be resumed for this cell. The disassembled cell showed cracks in the ceramic electrolyte, as well as macroscopic segregation of zinc metal towards the bottom of the cell.

For cell #3, we maintained a constant operating temperature of 300 °C and symmetric charge/discharge rates of C/15 (2.6 A) during the run-in procedure, avoiding an intermediate cycle at 240 °C (between 1.70 and 2.35 V, Fig. 7a). While the available capacity increased with each cycle, only 65% SOC (24.8 Ah) were reached after the first five cycles at 300 °C. Thus, cooling down for an intermediate cycle at 240 °C and consecutive reheating to 300 °C seems to have a positive effect on the cathode microstructure, thereby enabling cycling of the full capacity.

During consecutive regular cycling of cell #3 at a constant temperature of 300 °C (Fig. 7b, cycle 6–10), we first reduced the charge rate to C/29, but the capacity available during charge increased only slightly (from 68 to 69% SOC, Fig. 7c). Nevertheless, despite almost full discharge at C/15 (down to 1% SOC), the cell voltage remained stable, enabling cycling over 67±1% SOC (25.4 ± 0.2 Ah). While the charge times exceeded 21 h due to the low rate applied in cycle 6–10, the discharge times approached the CC limit of ~10 h (Fig. 7d). Due to the lower SOC range, the corresponding discharge energies were slightly lower than for cells #1 and #2 (202±2 Wh/kg), but the energy efficiency remained between 91% and 90% (Fig. 7e). In a next step, we performed two intermediate cycles at 240 °C and 300 °C, trying to charge the full capacity as in previous run-in procedures. However, this procedure increased the charge capacity only slightly, reaching 73% SOC in cycle 12 at 300 °C (27.8 Ah, see SI section G). This indicates that the cycling history significantly affects the resulting cathode microstructure. In a next step, we decreased the operating temperature for this cell to 280 °C, and performed 10 cycles at symmetric charge and discharge rates of C/15 (Fig. 7b, cycle 13–22). Possibly related to the intermediate cycle at 240 °C, the cell voltage at SOC >60% was lower at 280 °C than in the previous cycles at 300 °C, which enabled charging a higher capacity at the given cut-off voltages (up to 79% SOC, Fig. 7c). Both charge and discharge times varied between 12.0 and 13.5 h (Fig. 7d), slightly above the constant-current limit of ~11.5 h Related to the increase in cycled capacity (from ≈1–69% SOC at 300 °C to ≈2–79% SOC at 280 °C), the discharge capacity reached 231±3 Wh/kg (Fig. 7d, approximately linear increase from 226 to 236 Wh/kg). The corresponding energy efficiencies remained ≥90% at 100% coulombic efficiency (see SI section E), with only minor degradation of −0.1%/cycle, reaching a cumulative capacity of >550 Ah (>2.1 Ah/cm^2) after 22 cycles.

In line with the stable voltage profiles, postmortem analysis of cell #3 confirmed a homogenous cathode composition (Fig. 7f), which did

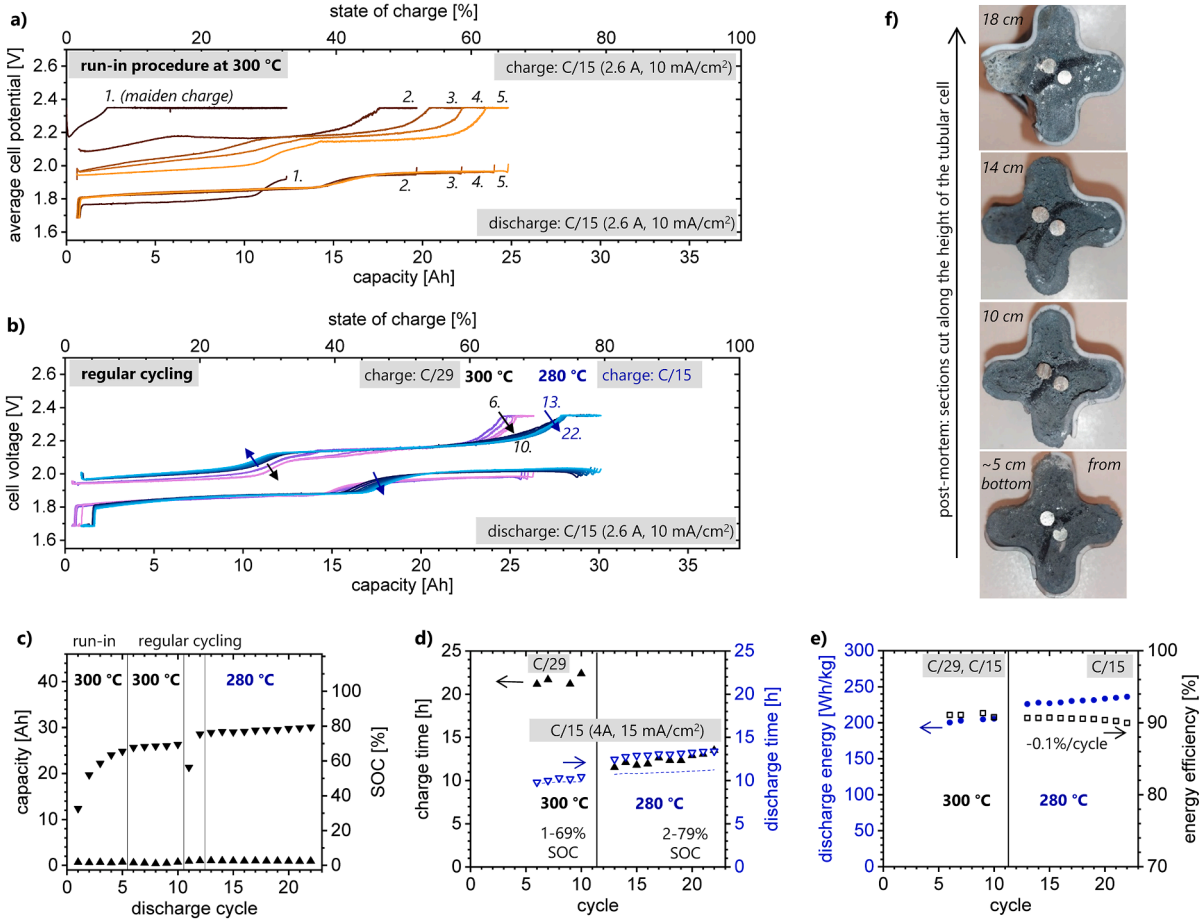

Fig. 7. Cycling of 3rd tubular Na-ZnCl$_2$ cell (37.9 Ah) at 300 °C between 1.70 and 2.35 V, cumulative capacity >550 Ah (2.1 Ah/cm^2). a) In the first 5 run-in cycles, the available capacity increases continuously from 12 Ah (33% SOC) to 25 Ah (66% SOC). b) During regular cycling at 300 °C (cycle 6–10) and 280 °C (cycle 13–22) the targeted charge/discharge range of 100% SOC (37.9 Ah) is not met. (Two intermediate cycles were performed at 240 °C and 300 °C, see SI section F). Nevertheless, c) the cycled capacity stabilizes between 1% and 69% SOC at 300 °C, and between 1% and 79% SOC at 280 °C. d) At 300 °C, charge times and discharge times amount to 21.6 ± 0.6 h and 10.2 ± 0.2, respectively. At 280 °C, charge and discharge times amount to 11.5 to 13.5 h d) The corresponding discharge energies and energy efficiencies amount to 202±2 Wh/kg, 91% at 300 °C, and to 231±3 Wh/kg, 90% at 280 °C. e) After cycling, no segregation is observed in the cathode material, but the ceramic electrolyte tube fractures upon sectioning.

not show apparent zinc metal segregation (as observed for cell #1, Fig. 4f). As cell #3 performed more cycles at elevated temperatures than cell #1 (22 vs. 14 cycles, 29 vs. 24 days at ≥280 °C, cumulative capacity >550 vs. 400 Ah), cycling to <80% SOC seems to stabilized the cathode microstructure, thereby providing a higher cycling stability. This could indicate that the Zn^{2+}-containing liquid phases formed at high SOC in Na-$ZnCl_2$ cells [6] affect both cathode microstructure and cycle life of cell #1, which is avoided by limiting the SOC range for cell #3. In this context, a higher density of Zn^{2+}-containing liquid phases, compared to $NaAlCl_4$, may cause aggregation of metallic zinc towards the bottom of cell #1 (Fig. 4f). However, the tubular Na-β''-alumina electrolyte of cell #3 fractured during sectioning. While reliable conductivity measurements could not be obtained on the small fragments, the stable voltage profiles during cycling indicate that the ceramic was not affected by a significant decrease in ion conductivity. Furthermore, phase changes of crystalline Na-β''-alumina were not detected in the electrolyte by X-ray powder diffraction, compared to pristine samples, neither for cell #1 nor #3 (Fig. 8, see SI section H for a split view on all patterns). Thus, we observe no direct signs of an exchange of Na^+ ions with Zn^{2+} in the Na-β''-alumina crystal structure after cell cycling. In any case, the electrochemical cycling data of cell #3 in Fig. 7 is not affected by electrolyte degradation. Related to the stability of the cathode structure, cycling to lower SOC enhanced the cycling stability of Na-$ZnCl_2$ cell #3, compared to cells #1 and #2. This could indicate that the phase content formed at the cathode at high SOC in the cells #1 and #2 has a detrimental effect on the relevant transport processes, thereby increasing the resistance contribution of the cathode. According to the phase diagram of NaCl and $ZnCl_2$ [6], zinc chlorination at 300 °C proceeds via formation of Na_2ZnCl_4 (0–50% SOC) and different salt melts, before solid $ZnCl_2$ is formed above 80% SOC. Our experiments suggest the electrochemical formation and dissolution of solid $ZnCl_2$ at high SOC to dominate the performance degradation of additive-free Zn/NaCl cathodes. Further studies are required to elucidate the mechanical, chemical, and electrochemical stability of Na-$ZnCl_2$ cells and possible degradation mechanisms in Na-β''-alumina.

5. Conclusions

Replacing nickel in the cathode of sodium-nickel chloride batteries by zinc could provide a cost-efficient and sustainable solution for large-scale energy storage. Energy storage prices as low as 0.02 $/kWh/cycle are possible, presuming sodium-zinc chloride (Na-$ZnCl_2$) batteries to provide a cycle life exceeding 4500 cycles, like state-of-the-art Na-$NiCl_2$ batteries. Furthermore, cells need to provide a high areal capacity in order to compensate the cost contributions for high-temperature cell components and manufacturing.

In this study, we first integrated Zn/NaCl electrodes into state-of-the-art tubular high-temperature cells at commercial scale. To avoid critical stresses on the ceramic electrolyte and to assure safe operation, we estimated the volume changes of electrode materials during cell cycling, and derived the resulting pressure difference between the electrode compartments. In this context, we identified cost benefits for an alternative inside-out cell design, which could provide twice the capacity of state-of-the-art cells (e.g. >80 Ah), without changing size and geometry of the ceramic Na-β''-alumina electrolyte and its seals. Placing the cathode towards the outside of tubular cells could significantly reduce the cost-contribution of cell components and assembly, without negatively affecting pressure difference in Na-$ZnCl_2$ cells during cycling.

Second, we demonstrated constant-current followed by constant-voltage cycling of an additive-free Zn/NaCl electrode with 30% active metal content (160 mAh/g) in state-of-the-art tubular cells with a capacity of 37.9 Ah capacity (146 mAh/cm^2, 0.9 g/cm^2). The available capacity in these cells depends on the operating temperature applied in the run-in procedure, while the stability of voltage profiles is dominated by the SOC range activated during cycling. When cycled between 12% and 96% SOC at 300 °C, these cells reached discharge energies of up to 260 Wh/kg at 15 mA/cm^2 (C/10, cell #2). However, cycling to high SOC (close to 100%) involved a continuous increase in cell resistance with each cycle, which decreased the energy efficiency by ~1%/cycle (at 15 mA/cm^2, C/10). In contrast, the cell voltage remained stable for cycling below 80% SOC. Under these conditions, a cumulative capacity of >550 Ah, 2.1 Ah/cm^2 was cycled, providing stable discharge energies of 231 ±3 Wh/kg at energy efficiencies ≥90%. Our experiments demonstrate how the detailed cycling history (including operating temperature, cut-off voltage, current density, and SOC range) affect the stability of Zn/NaCl electrodes. At the current stage, the stability of cathode materials limit the rate capability and cycle life of tubular cells, which may be enhanced by suitable additives and/or changes to the cathode microstructure. Further studies should address the chemical, electrochemical and mechanical long-stability of the ceramic Na-β''-Al_2O_3 electrolyte in the presence of zinc species at the cathode.

Questionnaire

Novelty

First demonstration of environmentally benign sodium-zinc chloride battery cells at commercially relevant scale (capacity 37.9 Ah/cell, 146 mAh/cm^2).

Important

Replacing the cathode metal in sodium-nickel chloride batteries by abundant zinc may enable sustainable energy storage for stationary applications at competitive costs of 0.02–0.04 $/kWh/cycle.

Why publish

We are convinced that our study will motivate further studies on this important topic, and serves as a step towards potential commercial application.

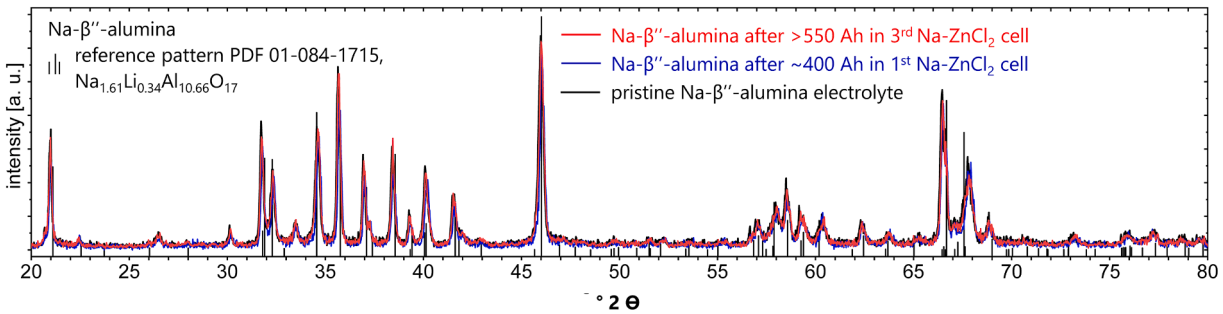

Fig. 8. The XRD phase content of the Na-β''-alumina electrolyte remains unchanged after cycling in Na-$ZnCl_2$ cells.

CRediT authorship contribution statement

Meike V.F. Heinz: Conceptualization, Methodology, Formal analysis, Writing – original draft, Visualization, Project administration, Funding acquisition. **Louis Sieuw:** Writing – review & editing. **Tu Lan:** Writing – review & editing. **Alberto Turconi:** Investigation, Validation. **Diego Basso:** Investigation, Supervision. **Fabrizio Vagliani:** Investigation. **Andrea Pozzi:** Project administration. **Corsin Battaglia:** Supervision, Writing – review & editing.

Declaration of Competing Interest

The authors declare that they have no known competing financial interests or personal relationships that could have appeared to influence the work reported in this paper.

Data availability

Datasets related to this article are available at doi.org/10.5281/zenodo.7357347.

Acknowledgements

This project has received funding from the European Union's Horizon 2020 research and innovation program under grant agreement No 963599 (SOLSTICE).

Supplementary materials

Supplementary material associated with this article can be found, in the online version, at doi:10.1016/j.electacta.2023.142881.

References

[1] G.L. Soloveichik, B.attery technologies for large-scale stationary energy storage, Annu. Rev. Chem. Biomol. Eng. 2 (2011) 503–527.
[2] M. Sufyan, N.A. Rahim, M.M. Aman, C.K. Tan, S.R.S. Raihan, Sizing and applications of battery energy storage technologies in smart grid system: a review, J. Renew. Sustain. Energy 11 (2019) 14105.
[3] FZSoNick, Sodium Metal Chloride Battery System, Technical overview, 2021. /08/31. Dowloaded from, www.fzsonick.com/home, 2023-01-03.
[4] European Commission, COMMITTEE AND THE COMMITTEE OF THE REGIONS Critical Raw Materials Resilience: Charting a Path Towards Greater Security and Sustainability. COM(2020), 4, Communication COM, 2020, pp. 1–24 (2020).
[5] P. Parthasarathy, N. Weber, A.V. Virkar, High temperature sodium - zinc chloride batteries with sodium beta - alumina solid electrolyte, ECS Trans 6 (2007) 67–76.
[6] X. Lu, et al., A novel low-cost sodium-zinc chloride battery, Energy Environ. Sci. 6 (2013) 1837–1843.
[7] X. Lu, et al., An Intermediate-temperature high-performance Na-ZnCl2 battery, ACS Omega 3 (2018) 15702–15708.
[8] Y. Lee, et al., Electrochemically activated Na–ZnCl2 battery using a carbon matrix in the cathode compartment, J. Power Sources 440 (2019), 227110.
[9] C.H. Dustmann, Advances in ZEBRA batteries, J. Power Sources 127 (2004) 85–92.
[10] T. Javadi, A. Petric, Thermodynamic analysis of reaction products observed in ZEBRA cell cathodes, J. Electrochem. Soc. 158 (2011) A700.
[11] D. Landmann, E. Svaluto-Ferro, M.V.F. Heinz, P. Schmutz, C. Battaglia, Elucidating the rate-limiting processes in high-temperature sodium-metal chloride batteries, Adv. Sci. 9 (2022), 2201019.
[12] B.V. Ratnakumar, A.I. Attia, G. Halpert, Sodiummetal chloride battery research at the jet propulsion laboratory (JPL), J. Power Sources 36 (1991) 385–394.
[13] J.L. Sudworth, The sodium/nickel chloride (ZEBRA) battery, J. Power Sources 100 (2001) 149–163.
[14] V. Zinth, et al., Neutron tomography and radiography on a sodium metal halide cell under operating conditions, J. Electrochem. Soc. 163 (2016) A838–A845.
[15] M.V.F. Heinz, G. Graeber, D. Landmann, C. Battaglia, Pressure management and cell design in solid-electrolyte batteries, at the example of a sodium-nickel chloride battery, J. Power Sources 465 (2020), 228268.
[16] G. Róg, A. Kozlowska-Róg, Divalent Ion-β″-Alumma electrolytes for the study of thermodynamic properties of oxide systems, Zeitschrift fur Phys. Chemie 207 (1998) 83–92.
[17] G. Róg, S. Koziński, A. Kozowska-Róg, Solid oxide galvanic cells involving exchanged beta-alumina electrolyte, Electrochim. Acta 26 (1981) 1819–1821.
[18] Yung-Fang Yu Yao, J.T Kummer, Ion exchange properties of and rates of ionic diffusion in beta-alumina, J. Inorg. Nucl. Chem. 29 (1967) 2453–2475.
[19] R.C. Galloway, S. Haslam, The ZEBRA electric vehicle battery: power and energy improvements, J. Power Sources 80 (1999) 164–170.
[20] D. Landmann, G. Graeber, M.V.F. Heinz, S. Haussener, C. Battaglia, Sodium plating and stripping from Na-β‘‘-alumina ceramics beyond 1000mA/cm2, Mater. Today Energy 18 (2020), 100515.
[21] J. Prakash, L. Redey, D.R. Vissers, M.orphological considerations of the nickel chloride electrodes for zebra batteries, J. Power Sources 84 (1999) 63–69.
[22] G. Graeber, et al., Rational cathode design for high-power sodium-metal chloride batteries, Adv. Funct. Mater. 31 (2021), 2106367.
[23] R.C. Galloway, C.-H. Dustmann, ZEBRA battery - material costavailability and recycling, EVS-20 19 (2003) 1–9. Nov. 15.
[24] Z. Wen, Y. Hu, X. Wu, J. Han, Z. Gu, Main challenges for high performance NAS battery: materials and interfaces, Adv. Funct. Mater. 23 (2013) 1005–1018.
[25] X. Wang, et al., Ni, Cr, and Fe surfaces corroded by molten ZnCl2, Mater. Corros. 71 (2020) 931–937.
[26] M.V.F. Heinz, M.C. Bay, U.F. Vogt, C. Battaglia, Grain size effects on activation energy and conductivity: na-β″-alumina ceramics and ion conductors with highly resistive grain boundary phases, Acta Mater 213 (2021), 116940.
[27] T. Lan, et al., Planar sodium-nickel chloride batteries with high areal capacity for sustainable energy storage, Adv. Funct. Mater. (2023), https://doi.org/10.1002/adfm.202302040.